Large-scale groundwater monitoring in Brazil assisted with satellite-based artificial intelligence techniques

Clyvihk Renna Camacho[1,2], Augusto Getirana[3,4], Otto Corrêa Rotunno Filho[2], Maria Antonieta A. Mourão[1]

1 Geological Survey of Brazil, Belo Horizonte, Brazil

2 Civil Engineering Department, Federal University of Rio de Janeiro, Rio de Janeiro, Brazil

3 Hydrological Sciences Laboratory, NASA Goddard Space Flight Center, Greenbelt, MD, United States

4 Science Applications International Corporation, Greenbelt, MD, United States

Abstract – Here, we develop and test an artificial intelligence (AI)-based approach to monitor major Brazilian aquifers. The approach combines Gravity Recovery and Climate Experiment (GRACE) data and ground-based hydrogeological measurements from Brazil's Integrated Groundwater Monitoring Network at hundreds of wells distributed in twelve aquifers across the country. We use a model ensemble composed of four different AI models: Extreme Gradient Boost, Light Gradient Boosting Model, CatBoost and Multilayer Perceptron. The approach is further boosted with wavelet and seasonal decomposition processes applied to GRACE data. To determine the sensitivity of the AI approach to data availability, we propose four experiments combining hydrogeological measurements from different aquifers. Groundwater storage estimates from the Global Land Data Assimilation System (GLDAS) are used as the benchmark. The AI approach successfully reproduces groundwater storage estimates at all Brazilian aquifers. Results show that the proposed approach outperforms GLDAS in all experiments, with an average Nash-Sutcliff efficiency of 0.91 and an average RMSE of 0.43cm for the experiment that covers all monitored wells in Brazil. GLDAS resulted in -1.311 and 5.84cm, respectively. This study demonstrates that combining satellite data and AI can be a cost-effective alternative to monitor poorly equipped aquifers at the continental scale.

Key Points

- An Artificial Intelligence (AI)-based model was built to monitor groundwater in Brazilian aquifers using satellite gravimetry data
- AI-based groundwater changes outperformed Global Land Data Assimilation System (GLDAS) estimates in all proposed experiments
- Results show that satellite-based AI techniques can be an effective solution for groundwater monitoring in poorly equipped regions

1 - Introduction

Proper aquifer monitoring at local, regional and large scale faces enormous difficulties to be achieved due the complexity and diversity of geological formations and the corresponding lithologic and facial structures, hydraulic properties, recharge zones and groundwater exploitation accentuated by land use and land cover changes coupled to meteorological and climatic variability. There is definitely a demand for global and operational hydrogeological monitoring, once groundwater is the largest unfrozen freshwater stock on the planet and tightly connected to surface water, reservoir and lakes (Condon et al., 2021). In 2002, over 1.5 billion people were estimated to be directly supplied by groundwater (Alley *et al.*, 2002). This number has risen to 2 billion people in 2020 (UNESCO, 2020). It is estimated that 43% of the total water used in irrigation has underground origin (Siebert et al., 2010). Countries such as the United States and India use approximately 25% and 40% of groundwater resources to supply their respective needs (Getirana et al., 2021), resulting in significant aquifer depletions (e.g., Rodell *et al.* 2018; Nie *et al.* 2019). In Brazil, about 57% of its municipalities have groundwater supply to some extent (IBGE, 2020). The intensification of groundwater use, combined with the impacts of climate change, has been causing the depletion of aquifers worldwide (Richey et al., 2015). Therefore, it is essential to understand groundwater spatiotemporal dynamics to ensure its sustainable use.

Groundwater monitoring networks have been based on observation wells associated with the creation of conceptual and mathematical models (Condon et al., 2021). Large-scale hydrological model outputs, such as those produced by the Global Land Data Assimilation System (GLDAS; Rodell et al., 2003), can be used as an alternative to the absence of hydrogeological monitoring systems. Such modeling systems can explicitly represent, in a simplified way, groundwater dynamics (Getirana et al., 2020; Li et al., 2019). Such models are robust in their structure and have the ability to provide the behavior of surface water and groundwater at continental and global scales. However, these models still need to be adjusted for optimal regional use (Getirana et al., 2020).

A new frontier has been opened for the study of groundwater by gravitational data provided by the Gravity Recovery and Climate Experiment (GRACE) (Tapley et al., 2004) and GRACE Follow On (GRACE-FO) missions, which measure changes on global gravitational forces. Among those changes, there are those promoted by the water cycle. They can be mapped by satellites and later converted into terrestrial water storage (TWS)

variability. Several studies have used data from GRACE missions to capture regional groundwater behavior and to assess measurements related to groundwater levels (Andrew et al., 2017; Frappart and Ramillien, 2018; Getirana et al., 2020; Scanlon et al., 2012, 2018). In Brazil, the use of GRACE data to understand the water behavior can be found in recent studies (Getirana, 2016; Hu et al., 2017; Gonçalves et al., 2020; Getirana et al., 2021). Li et al. (2019) assimilated GRACE data into a hydrological model globally and analyzed groundwater variations, comparing model results to *in situ* observations.

There is a clear contribution of GRACE data assimilation (DA) into hydrological models in the representation and prediction of hydrological processes (Getirana et al., 2020; Getirana et al., 2020; Girotto et al., 2017; Jung et al., 2019; Kumar et al., 2016). Nevertheless, new tools based on the so-called artificial intelligence (AI) algorithms have also proved to be very efficient for the pattern recognition of groundwater behavior worldwide (Afzaal et al., 2020; Huang et al., 2019; Iqbal et al., 2021; Lähivaara et al., 2019; Ren et al., 2021; Tao et al., 2022; Zhang et al., 2020).

AI algorithms, associated with GRACE-based TWS variations can be of great value in the survey of aquifers. Groundwater studies using AI and GRACE data have been carried out for some years (Gemitzi and Lakshmi, 2017; Sun, 2013; Sun et al., 2019). Wave decomposition methods are also very useful in hydrological studies for flow prediction, seasonal analysis or even hydrogeological studies (Ashraf et al., 2022; Basu et al., 2022; Erkyihun et al., 2016; Qi and Neupauer, 2008). Hybrid use of AI and wavelet decomposition techniques turned out to be an important and active research area, resulting in more accurate models in water resources applications, due to its great ability to discriminate non-stationary and nonlinear trends that occur at different scales in groundwater time series (e.g., Tao et al., 2022). For example, Andrew et al. (2017) presented the possibility of disaggregating GRACE data using wavelets as a viable path to study groundwater under different observational spatiotemporal scales.

Brazil's Integrated Groundwater Monitoring Network (RIMAS), conceived and built by the Geological Service of Brazil, initiated in 2010 and is currently composed of 409 wells, monitoring 24 aquifers across the country. The distribution of wells across the monitoring network is not homogeneous, leading to constraints in monitoring the spatiotemporal variability of the nation's aquifers. Also, only porous, free or semi-confined aquifers have been monitored by RIMAS. Such a sparce network is substantially less dense than those found in other large countries, such as the U.S. and India, which

have more than 16,000 and 22,000 wells, respectively (Getirana et al., 2021). That leads to limited groundwater monitoring in Brazil. The limited knowledge on Brazil's groundwater dynamics limits management and optimized use of its aquifers. The absence of data also limits the development and parameterization of hydrological and hydrogeological models to monitor Brazil's water resources, resulting in inaccurate water flow and storage calculations, affecting various sectors of society such as agriculture, energy generation and domestic supply (Getirana et al., 2021).

Considering the limitations described above, this work presents a methodology that combines point-based *in situ* groundwater measurements and spatially-distributed satellite-based TWS, in addition to wavelet decomposition techniques and artificial intelligence (AI) as tools to understand the behavior of large aquifers in Brazil. The main advantage of the proposed methodology is the use of a hybrid model (wave decomposition + ensemble model) with the application of four different AI techniques. GLDAS-based groundwater simulations are used as the benchmark to determine the potential of the proposed methodology. GLDAS simulations are those derived from the Catchment Land Surface Model (CLSM) (Koster et al., 2000) with GRACE-DA (Li et al., 2019). We considered such simulations as our benchmark because they have been comprehensively evaluated globally and are widely used. Also, it is currently the only temporally continuous and spatially distributed groundwater product available in Brazil. We expect that the proposed methodology can be used for the management of large Brazilian aquifers, in addition to enabling the monitoring of groundwater in places where monitoring networks are precarious, inexistent, or with heterogeneous hydrogeological and climatic conditions.

2 – Case study and Datasets

2.1 – *In situ* data from aquifers

Aquifers monitored by RIMAS total 2,839,558km^2, or 34% of the Brazilian territory. Their sizes vary from 884km^2 (Missão Velha) to 774,385km^2 (Içá), with monitoring coverage varying from 3 (Ronuro) to 71 (Urucuia) wells. Their spatial distribution and RIMAS network are shown in Figure 1. The monitoring network density varies significantly, with Missão Velha being the aquifer with the highest density of wells (0.018 wells/km^2) and Içá with the lowest density (0.000013 wells/km^2). Such a heterogeneous density is mostly explained by the way the network is installed, which as initial criteria: sedimentary aquifers, socioeconomic importance of the water, water use

for public supply, natural vulnerability and risk aspects, spatial representativeness of the aquifer and existence of wells for monitoring (Mourão, 2009). Effective porosity (S_y) values for each aquifer were estimated based on available data found in the literature (please refer to Table 1 for a full list), varying from 0.03 in Cabeças Aquifer to 0.18 in Alter do Chão Aquifer.

RIMAS is designed based on wells equipped with automatic level meters collecting data at the hourly step, which are subsequently subjected to consistency, treatment, and availability processes (http://rimasweb.cprm.gov.br/layout/). The estimated error of the measurements is the minimum resolution of the equipment, which varies between 0.01 and 1.5 cm. More specifically, porous, free, semi-confined and wells in areas of crystalline rocks are addressed in this study, focusing on the responses that different lithologies might produce and how that information could be translated into the building AI model approach we are developing in-here. Geological and hydrogeological description of the aquifers monitored by RIMAS can be found at http://rimasweb.cprm.gov.br/layout/apresentacao.php.

The RIMAS dataset is available at the hourly time step. Monthly groundwater level change (dh_i) at each well was computed by first converting the time series to monthly means, then subtracting the value in the previous month (η_{i-1}) from the subsequent one (η_i), as follows:

$$dh_i = \eta_i - \eta_{i-1} \quad (1)$$

Where i stands for months of the time series. Each dh_i value was then subtracted by their respective long-term mean, and multiplied by their corresponding aquifer S_y value, resulting in the time series used as input in our approach, named hereafter as GWS_{OBS}(cm). S_y was used in order to normalize time series at all wells, from groundwater level to storage equivalent. Equation 2 shows the calculation of GWS_{OBS} (cm) for each month i:

$$GWS_{OBS}(i) = [dh_i - \text{mean}(dh)].S_y \quad (2)$$

2.2 - Terrestrial water storage

GRACE RL06 Mascon data, processed by the Center of Space Research (CSR; Save et al., 2016), is retrieved at 0.25-degre spatial resolution and monthly time step from

April, 2002 to present with gaps throughout the period. Initially, monthly GRACE-based TWS values had uncertainties estimated at 1cm for areas equal to or greater than 400,000km^2 (Swenson et al., 2003). However, such estimates had a significant improvement, as described in Ditmar (2018), obtaining more refined results for TWS approximations at 0.25-degree spatial resolution. Such Mascon-based products have lower errors compared to spherical harmonics (Rowlands et al., 2010). Even maintaining a resolution limited by the nature of the GRACE data and uncertainties in the TWS of 1cm, these estimates allow a more detailed study of hydrological and hydrogeological basins with dimensions smaller than those indicated by Save (2020) as demonstrated in Melati et al. (2019) and Gonçalves et al. (2020), both carried out in Brazil.

2.3 – GLDAS-based groundwater

The CLSM with GRACE-DA was chosen among the different GLDAS products for presenting an explicit and more accurate representation groundwater storage (GWS). CLSM is a state-of-the-art energy and water balance model of the Earth's surface, designed for use in models of global earth systems. The model simulates a dynamic water table with a spatial distribution related to the topography of the basin (Bechtold et al., 2019). Details about the model configuration and global evaluation can be found in Li et al. (2019).

3 – Methodology

Briefly, the methodology follows four steps. First, wave decomposition (wavelet and seasonal) on the TWS values for Brazil. Second, interpolation of the values obtained by the wavelets for the original time scale. Third, the decomposition results are associated with the RIMAS measurements, according to latitude, longitude and time. Hydrogeological data of the Hydrogeological Map of Brazil (HMB) is also associated with RIMAS wells according to latitude and longitude. Finally, the dataset is inserted into an AI model to approximate the groundwater storage (GWS_{OBS}) values obtained by the RIMAS wells. The input values in the model are: TWS values, decompositions (wavelet and seasonal), hydrogeological description of the HMB in addition to the latitude and longitude values of wells. Groundwater storage estimates from the CLSM GRACE-DA (GWS_{CLSM}) are used as the benchmark.

Wavelet transform is a technique that has proven to be effective for capturing nonlinear relationships in time series (Tao et al., 2022). It removes noise in the data and

allows a better performance in AI models. Several hydrogeological studies have combined these techniques and demonstred the ability to approximate variations in groundwater levels from different data sources (Barzegar et al., 2017; Ebrahimi and Rajaee, 2017; Khalil et al., 2015; Moosavi et al., 2014, 2013; Yosefvand and Shabanlou, 2020; Zare and Koch, 2018). Here, GRACE-based TWS was decomposed using two techniques: the wavelet transform and the seasonal decomposition.

Wavelet transform (WT) is a mathematical tool to decompose functions hierarchically, and can be considered as a technique for transforming a signal, sampled in the time domain, into a frequency-scaled domain, defining different components of the signal frequency spectrum (Stollnitz et al., 1995). WT consists of approximating a function by a linear combination of basic functions (also called wavelets), obtaining a representation of the original function. The application of wavelets does not necessarily require the stationarity of the time series as a prerequisite, being appropriate for the analysis of irregularly distributed and extreme events (Torrence and Compo, 1998). For non-continuous functions, the use of the discrete wavelet decomposition (DWT) is recommended (Daubechies, 1992), as in the case of this study.

To apply the wavelet transform, the highest possible decomposition level of the TWS signal was tested, resulting in five levels. The wavelet family chosen for the decomposition was db3 (Daubechies, 1992). The signal extension model was observed, seeking the best possible application of DWT. The data normalization mode adopted for the WT was the *antireflect*, signal is extended by reflecting anti-simmetrically about the edge sample (PyWavelets, 2022). After decomposing the TWS with DWT, the results are a sequence compressed in one of the dimensions. As the TWS is being treated in three dimensions (i.e., latitude, longitude and time), and decomposed into the time dimension, the transform results reduce the time dimension. The time scale reduction occurs because DWT employs a grid where the mother wavelet is scaled by power two, expressing the results of each decomposition level as half of the previous level (Rhif et al., 2019). As the TWS input data has 194 data points per time series, DWT returns the approximation values A5 (194 values) and details, namely D1 (96 values), D2 (48 values), D3 (24 values), D4 (12 values) and D5 (6 values). To return the time dimension to the original scale of the decomposition, an interpolation model in *Spline* was applied. This method adapts a smooth variation of values for locations without data. This procedure requires the application of a mathematical function that minimizes the curvature of the surface,

obtaining a result where the response is smooth and the surface passes exactly through the given entry points (Marcuzzo et al., 2012).

TWS time series has also passed through the seasonal decomposition method, which returns a moving average around an established window value. The chosen window size was 12 months, seeking to observe the annual variations in the data. The model is additive and suggests that the components are added together as follows (Perktold et al., 2022):

$$TWS_{[t]} = T_{[t]} + S_{[t]} + e_{[t]} \quad (3)$$

The results are represented in three outputs at each time step [t], seasonality (S), trend (T) and residual (e). T is an increasing or decreasing value in the series, S is the short-term repetitive cycle in the series, and e is the random variation of the series.

Hydrogeological characteristics of aquifers obtained from the Hydrogeological Map of Brazil (Diniz et al., 2014) were inserted into the model. The characteristics observed in each well were as follows: geological group, lithological description of the group, the type of aquifer, the degree of fracturing and the productivity of the aquifer. These non-numerical data were converted into zero and one values (0, 1) by the *one-hot* function (Scikit-learn, 2021) to be better used in the model.

3.1 - Ensemble model

The ensemble model is composed of four different AI models, three of which use the Decision Tree (DT technique); the Extreme Gradient Boost (XGB; Chen and Guestrin, 2016), the Light Gradinet Boosting Model (LGBM; Ke et al., 2017) and the CatBoost (CtB; Prokhorenkova et al., 2017), followed by an Artificial Neural Network, Multilayer Perceptron (MLP; Manaswi, 2018). Figure 2 shows the data processing flow and the architecture of the ensemble model. The input data in the model are the TWS, decompositions (wavelet and seasonal), the hydrogeological characteristics depicted by the hydrogeological map and the position of the well in space (latitude and longitude). The extreme values are removed from the input dataset by quantile threshold evaluation, respecting the criteria of being greater than 99% and less than 1% of the GWS_{OBS}. Finally, the data are normalized. It should be noted that the GWS_{OBS} values are not normalized. After the initial processes, the data are inserted into the DT models for the first approximations of the GWS_{OBS} values from the input data. The results obtained after

processing in the DT models are then inserted into the MLP that finalizes the approximations of the GWS_{OBS} observed in the wells. The ensemble model application uses the AI premise that weak models joined together can build a stronger model (Géron, 2019).

The architecture of the AI models used was:

XGB: estimators 3000; learning rate 0.001; sampling set 1; maximum depth 7; *XGBRegressor – gbtree*; early stop 150 steps.

LGBM: regression *boosting_type gbdt*; l1 and l2 metrics; learning rate of 0.001; layer fraction of 0.9; *bagging_fraction* 0.7; *bagging_freq* 20; maximum depth 8; number of sheets 128; *max_bin* 512; number of interactions 3000; early stop 150 steps.

CtB: number of iterations 3000, learning rate 0.01, depth 7, RMSE rating metric, *bagging_temperature* 0.01, *od_type*: Iter and *od_wait*: 20.

MLP: *Selu* activation functions in the input layer with 128 neurons and *Swish*; in the others, with 256/256/128 neurons; 10000 epochs; between the hidden layers the functions *Dropout* (0.2) and *GaussianNoise* (0.5); *LazyAdam* optimizer; with a reduction in the learning rate over time; 150 steps early stop.

For MLP, the *Swish* activation function (Ramachandran et al., 2017) was used because it presents great empirical performance. The *Selu* function or Scaled Exponential Linear Unit (Klambauer et al., 2017) was selected for inducing properties of self-normalization in the data; this function allows training deep networks with many layers, employing strong regularization schemes and making the learning highly robust. Finally, the optimizer chosen was *LazyAdam*, which is a stochastic gradient descent method. This optimizer is adapted from the *Adam* method (Kingma and Ba, 2015), which in turn combines the advantages of two methods, *AdaGrad* (Duchi and Singer, 2011) and *RMSProp* (Hinton et al., 2012). *AdaGrad* works well with sparse gradients, and *RMSProp* shows good results for non-stationary configurations.

The data entered in the models are divided into two sets. The first with 80% of the data for training/testing the model and the second with 20% of the data for blind testing the model, noting that the second batch was selected from the initial data set at random. In the first batch of data, for separating training from testing, 80% of the data is for training and 20% for testing the models during processing. After training and testing with

the first batch, the model is retested with the blind test wells. This procedure was performed to observe the real capacity of the model to adapt to different data sets.

The hyperparameters of the models had their initial adjustment by the Hyperactive algorithm (Blanke, 2021). However the final adjustment was done manually. We chose to use cross-validation (*K-Fold*) with ten (k=10) non-random subsets. Cross-validation is used to measure the accuracy of a model. The method consists of dividing the dataset into k mutually exclusive subsets of the same size and, from there, one subset is used for testing and the remaining k-1 are used for error estimation (Sklearn, 2022).

3.2 Evaluation of the ensemble model

The RIMAS network monitors the largest porous aquifers in Brazil, as illustrated in Figure 1. To assess the ability of the model proposed in this work to approximate the values of GWS_{OBS} observed *in situ*, the error analysis statistical metrics described in this section were used. However, in seeking a realistic comparison for the study areas with results obtained from a robust and widely tested model, the GWS results obtained from the CLSM model with GRACE-DA (GWS_{CLSM}), were used as baseline. For a comparison of the results obtained by the proposed ensemble model with GWS_{CLSM} and *in situ* data, four experiments were carried out, all using the same model described in the previous section. The experiments were designed to observe the model's ability to adjust to different datasets, training and test batch sizes, and different hydrological and hydrogeological conditions.

Experiment E1 – RIMAS and GRACE data used in Li et al. (2019), plus data obtained from the HMB. For this experiment, 60 wells with 4504 monthly *in situ* measurements were used.

Experiment E2 – In this experiment, all wells contained in the RIMAS database with more than 24 months of measurements were analyzed, as well as GRACE-based TWS and HMB data referring to the wells. In this experiment, 373 wells were used, resulting in 16,487 monthly *in situ* measurements.

Experiment E3 - RIMAS and GRACE data used in the work by Li et al. (2019), plus the data obtained from the MHB and separating the wells by monitored aquifer. Eight aquifers were selected, as follows: Alter do Chão, Parecis, Urucuia, Bauru-Caiuá, Guarani, Cabeças, Poti and Serra Grande. The Cabeças, Poti and Serra Grande aquifers were included in the same model as Poti and Serra Grande present similar effective

porosity (S_y) and close spatial distribution, renamed Cabeças/Serra Grande. Experiment 3 was not performed in the Içá, Missão Velha, and Mauruti aquifers, as there are only two wells in this aquifer in the dataset used by Li et al. (2019), which made it not possible to execute the model.

Experiment E4 - In this experiment, all wells contained in the RIMAS database with more than 24 months of measurements were analyzed, in addition to the GRACE and HMB data referring to the wells. Data were separated by monitored aquifer. Eleven aquifers were selected, as follows: Alter do Chão, Parecis, Urucuia, Bauru-Caiuá, Guarani, Cabeças, Poti, Serra Grande, Içá, Missão Velha and Mauruti. As in experiment E3, the Cabeças, Poti and Serra Grande aquifers were included in the same model as Poti and Serra Grande present similar effective porosity and close spatial distribution. The same procedure was performed for the Missão Velha and Mauruti aquifers, included in the same model, as they have a very close spatial distribution, wells in the same GRACE pixel, renamed as Araripe.

In experiments E3 and E4, not all monitored aquifers were addressed, as the number of wells used in the work by Li et al. (2019) is very small or non-existent in several of them. However, aquifers were selected in all regions of Brazil. It is important to emphasize that the input data in the model is related to the RIMAS data in spatial (*pixel*) and temporal scales, since each input data in the model has as reference the location of a well on a given date.

Cross-validation (*K-Fold*) was applied only in E1 and E2, due to the limited amount of data for training in E3 and E4.

As statistical metrics adopted for error evaluation across all experiments, the mean absolute error (MAE) (Equation 4), the root mean square error (RMSE) (Equation 5) and the Nash-Sutcliffe Efficiency (NSE) (Equation 6), were selected. For MAE and RMSE, the ideal values are zero. For the NSE, values closer to one indicate a better adjusted model.

$$\mathrm{MAE} = \sum_{i=1}^{n} |x_i - y_i| \quad (4)$$

$$\mathrm{RMSE} = \sqrt{\frac{\sum_{i=1}^{n}(x_i - y_i)^2}{n}} \quad (5)$$

$$\mathrm{NSE} = 1 - \frac{\sum_{i=1}^{n}(x_i - y_i)^2}{\sum_{i=1}^{n}(x_i - \bar{y}_i)^2} \quad (6)$$

where x_i stands for the *in situ* measurements, y_i the estimated values by the model, $\bar{y}_i$ the average of the model estimates, and *n* is the number of observations.

4 - Results and Discussion

4.1 Experiments E1 and E2

In experiments E1 and E2, the small errors were concentrated in the central and northeastern region of Brazil (Figure 3a, 3b), areas with a greater number of wells, while the largest errors were concentrated in the northern portion of the country, where there are fewer RIMAS wells inserted into the models. In general, the model built for experiments E1 and E2 presented MAE < 2 cm and RMSE < 3 cm (Figure 3a, 3b).

An interesting aspect that draws special attention in examining such results is the ability of the model to simulate the values of GWS_{OBS} in wells inserted in an environment of crystalline rocks, presented in the results of E2 (Figure 3b), southeastern region of Brazil. Despite the great variability of the GRACE signal in both experiments E1 and E2, which used data from all regions of Brazil, the average results show the great approximation of the simulated values GWS_{SIM} and GWS_{OBS} (Figures 3c to 3f), demonstrating the low variance of the presented results achieved by the constructed model. NSE values for E1 and E2 were 0.80 and 0.65, respectively (Figures 3a, 3b), indicating a good fit of the models to the datasets. However, those results make clear that not all the dependent variables were explained with precision. On the other hand, the low RMSE and MAE values show that the prediction errors presented for large areas are much lower than those derived from GWS_{CLSM} (see Table 2).

The cross-validation result (*K-Fold*) shows values very close to the complete model. For E1, NSE = 0.78, RMSE = 2.01 and MAE = 1.30. For E2, results are NSE = 0.64, RMSE = 2.67 and MAE = 1.68. Artificial intelligence models tend to perform better with larger batches of training and testing (Lecun et al., 2015). Due to the large

concentration of data in the central and northeast regions of Brazil, the model may have presented a biased result (Figure 3a, 3b), that is, with a tendency to present better results in areas with greater amount of data. In addition, there is a greater variability of GRACE signals in the north of the country.

As for the variability of the GRACE signal, it is expected that groundwater will present a different participation in each region of Brazil and in each aquifer studied. Signal variability is related to the hydrological processes of each region, as well as types, cover and land use. The northern region of Brazil has large bodies of surface water such as the Tocantins, Solimões, Negro and Amazon rivers, in addition to extensive floodable areas in the Amazon region, indicating a large contribution of surface water to the region's TWS signal (Getirana et al. 2017; Melo and Getirana 2019). Unlike the northern region and the swamps of the Brazilian Pantanal, the other regions of the country have a smaller amount of large surface water bodies. Even with the water filled up reservoirs built for the hydroelectric plants in these regions, a smaller component of surface water in the TWS signal is expected. Complementarily, these areas other than the northern regions have a higher groundwater extraction rate compared to the northern region of Brazil (IBGE, 2020). These factors may help to explain greater errors in the northern region of Brazil.

4.2 Experiments E3 and E4

Experiment E4 denotes that the highest values for RMSE are in Alter do Chão (Figure 4b), Parecis (Figure 4h) and Guarani (Figure 4f) aquifers. Although featuring RMSE values of 3.11 cm and MAE of 2.36 cm, Alter do Chão aquifer has an NSE value of 0.89. This result may occur due to the proximity of the wells to the Amazon River, which would affect the static water level fluctuations according to the water level variation of the river. In addition, many of these wells are inserted in an urban context, where land use and land cover jointly with underground water exploitation water can interfere in the results achieved by the models.

In the case of the Parecis aquifer, RMSE, MAE and NSE are 2.4cm, 1.36cm and 0.90, respectively. Uncertainties might be related once more to groundwater pumping, as the region has witnessed an increasing agricultural expansion in the past several years (IBGE, 2020).

For the Guarani aquifer, the variability of the GRACE signal associated with extraction processes might have hindered the best convergence of the models. The aquifer extends over thousands of kilometers and has experienced increasing groundwater pumping in its recharge areas for many years, as described by Takahashi (2012).

Areas with a higher concentration of monitoring wells return lower error values for each aquifer. Such a relationship is more visible in the results for the Cabeças/Serra Grande aquifers (Figure 4c) and Urucuia (Figure 4e). Errors of the test wells present lower values in these areas. Içá and Alter do Chão aquifers do not have as much data for training, resulting in model errors. However, results of all the aquifer models still return GWS_{SIM} values better than GWS_{CLSM}.

As noted by Brookfield et al. (2018), linear correlation analyses do not have the ability to extract from the TWS data relationships of water level variations of *in situ* measurements in areas with large vadose zones, areas that present greater depth of the static level. Different from the non-linear model presented in-here. This is highlighted in the responses of the ensemble model proposed and used in this work, mainly for the Urucuia aquifer (Figure 4e), an area of significant groundwater extraction and deep static water levels. Our model also has the ability to provide accurate estimates over areas with low thickness of the vadose zone and with great influence of surface waters, as observed in the wells present in the Içá (Figure 4a) and Alter do Chão (Figure 4b) aquifers.

The difference in scale between satellite data and *in situ* measurement data is addressed in many works, which may use statistical, dynamic methods (Gaur and Simonovic, 2019; Sehgal et al., 2021; Yin et al., 2018) and more recently artificial intelligence (Ali et al., 2021; Liu et al., 2020; Miro and Famiglietti, 2018). This issue was well solved by our model, as demonstrated in the results. Results are above expectations in the Araripe aquifer (Figure 4d), with RMSE, MAE and NSE of 0.24cm, 0.88cm and 0.88, respectively. This shows that aquifers inserted in a small area and wells in the same GRACE pixel were not a problem for the approximations made by the model.

Experiment E4 (Figure 5) indicate that, when the input data is concentrated in the same aquifer (e.g., Guarani, Urucuia and Bauru aquifers), estimated groundwater storage change less, which is expected due to the lower variability of the TWS signal, as well as constant geological characteristics of the aquifer under study. However, there were small gains, which can be explained by the amount of training data for the models.

Figure 5 shows the average observed and simulated (CLSM and our approach) GWS in the Guarani, Bauru-Caiuá and Urucuia aquifers. For the Guarani aquifer, experiment E4 shows that the model can predict with good accuracy the average behavior of the wells. It is worth noting that the test wells show a better result than GWS_{CLSM} (Figure 5). However, these wells depict a deviation from the expected response obtained for the wells included in the blind group for testing, which could indicate that the number of values for training the series might have directly interfered in the result. In the Bauru-Caiuá aquifer, the model presents results very close to RIMAS measurements (Figure 5).

The model's response could be associated with the spatial distribution of the RIMAS monitoring wells within the aquifer (Figure 4g), which covers almost the entire aquifer with a relatively constant spacing between the wells. In this aquifer, it is possible to notice that the model can approximate with great precision the RIMAS values for E4.

For experiment E3, the response is superior to that derived from GWS_{CLSM}, even with a high RMSE. This may have occurred because the wells included in this experiment are concentrated in an area of intense underground water extraction.

For the Urucuia aquifer, the behavior of adherence between AI model and measurements is superior to that of Bauru-Caiuá, however the great variability of the GRACE-based TWS estimates at each studied point, associated with different responses in each monitoring well to the groundwater extraction processes in the region, might contribute to a small departure of the predicted data with respect to the data measured by RIMAS in the blind test, even though this area presented the best results in the study (Figure 5). The small variation of the GWS observed and the one estimated by the model could indicate a constant loss of water along the column in the aquifer, as reported by the work of Gonçalves et al. (2020).

5 – Conclusions and recommendations

Here, we demonstrate the viability of satellite-based monitoring of Brazilian aquifers. A novel artificial intelligence model was conceived and built by employing GRACE-based TWS data and its decomposition using wavelet and seasonal techniques, jointly with point-based *in situ* hydrogeological data. As a benchmark for our results, we used GLDAS outputs, specifically, groundwater simulations derived from the CLSM model with GRACE data assimilation (GWS_{CLSM}). Results of the proposed methodology

over all selected aquifers showed accurate groundwater estimates, overperforming GLDAS estimates.

The TWS signal decomposition process proved to be very useful for the model, which adequately approximates the variations in groundwater storage in the different experiments. The proposed methodology can be applied in areas with a short history of groundwater monitoring and discontinuous time series, since aquifers such as Parecis, Içá and Cabeças/Serra Grande have less than ten years of static water level measurements and all wells in the RIMAS have gaps in their time series.

It is important to emphasize that the proposed models are representing the sample space inserted in the dataset. The big difference between the scales of the GRACE data with a resolution of 0.25° and *in situ* RIMAS measurements collected at an approximate point scale, were overcome by the models. Furthermore, more than one well per pixel was also not a problem, demonstrated by the results for the aquifers Içá, Parecis, Araripe and Urucuia. It is expected that the proposed model can be applied in areas with physical and geological characteristics similar to the training region, since the response of GRACE-based TWS signals tend to be similar. This feature can help to spatialize the storage of groundwater to unmonitored areas, being very useful for large aquifers.

As a model constraint, aquifers without a history of groundwater monitoring are difficult to approximate. Regions with great variation in physical characteristics, such as soil type, geology, land use and occupation, precipitation rates or groundwater extraction, can create situations in which the proposed model does not respond as expected. Another limitation of the model is the spatial resolution for unmonitored areas, which initially depends on the resolution of the GRACE data. In experiment E2, some wells are inserted in an environment of crystalline rocks. Despite the good results, the model has not yet been properly adjusted for this geological environment, as well as for karstic aquifers, being the subject of future investigation.

Groundwater monitoring using satellite data and artificial intelligence can be a solution to spatialize groundwater storage values with good accuracy. Additionally, it is possible to make predictions for storage in different scenarios and with low computational costs, modifying only TWS values. This approach can also help in understanding aquifer dynamics, since, after the initial adjustments, the model can evaluate the past groundwater behavior using the GRACE data that started in 2002.

Acknowledgements

This work was funded by the Brazilian Coordination for the Improvement of Higher Education Personnel (CAPES) and the Brazilian Council for Scientific and Technological Development (CNPq). GRACE data is available at http://www2.csr.utexas.edu/grace/RL06_mascons.html, GLDAS data is available through the Goddard Earth Sciences Data and Information Services Center (https://disc.gsfc.nasa.gov/), and *in situ* groundwater measurements are available through the RIMAS website (http://rimasweb.cprm.gov.br/layout/).

References

Afzaal, H., Farooque, A.A., Abbas, F., Acharya, B., Esau, T., 2020. Groundwater estimation from major physical hydrology components using artificial neural networks and deep learning. Water (Switzerland) 12. https://doi.org/10.3390/w12010005

Aguiar, C.J.B., Mourão, M.A.A., 2012. Relatório diagnóstico aquífero Alter do Chão no Estado do Amazonas. Bacia sedimentar do Amazonas. Manaus.

Aguiar, R.B. de, 2017. Caracterização Sistemática do Aquífero Serra Grande na Porção Nordeste da Bacia Sedimentar do Parnaíba. Universidade Federal do Ceará.

Ali, S., Liu, D., Fu, Q., Cheema, M.J.M., Pham, Q.B., Rahaman, M.M., Dang, T.D., Anh, D.T., 2021. Improving the Resolution of GRACE Data for Spatio-Temporal Groundwater Storage Assessment. Remote Sens. 13, 3513. https://doi.org/10.3390/rs13173513

Alley, W.M., Healy, R.W., LaBaugh, J.W., Reilly, T.E., 2002. Flow and storage in groundwater systems. Science (80-.). 296, 1985–1990. https://doi.org/10.1126/science.1067123

Andrew, R., Guan, H., Batelaan, O., 2017. Estimation of GRACE water storage components by temporal decomposition. J. Hydrol. https://doi.org/10.1016/j.jhydrol.2017.06.016

Ashraf, F. Bin, Haghighi, A.T., Riml, J., Mathias Kondolf, G., Kløve, B., Marttila, H., 2022. A Method for Assessment of Sub-Daily Flow Alterations Using Wavelet Analysis for Regulated Rivers. Water Resour. Res. 58. https://doi.org/10.1029/2021WR030421

Barzegar, R., Fijani, E., Moghaddam, A.A., Tziritis, E., 2017. Forecasting of groundwater level fluctuations using ensemble hybrid multi-wavelet neural network-based models. https://doi.org/10.1016/j.scitotenv.2017.04.189

Basu, B., Morrissey, P., Gill, L.W., 2022. Application of nonlinear time series and machine learning algorithms for forecasting groundwater flooding in a lowland karst area. Water Resour. Res. https://doi.org/10.1029/2021WR029576

Bechtold, M., De Lannoy, G.J.M., Koster, R.D., Reichle, R.H., Mahanama, S.P., Bleuten, W., Bourgault, M.A., Brümmer, C., Burdun, I., Desai, A.R., Devito, K., Grünwald, T., Grygoruk, M., Humphreys, E.R., Klatt, J., Kurbatova, J., Lohila, A., Munir, T.M., Nilsson, M.B., Price, J.S., Röhl, M., Schneider, A., Tiemeyer, B., 2019. PEAT-CLSM: A Specific Treatment of Peatland Hydrology in the NASA Catchment Land Surface Model. J. Adv. Model. Earth Syst. 11, 2130–2162. https://doi.org/10.1029/2018MS001574

Blanke, S., 2021. Hyperactive: An optimization and data collection toolbox for convenient and fast prototyping of computationally expensive models. [WWW Document]. GitHub. URL https://github.com/SimonBlanke/Hyperactive (accessed 11.11.21).

Brookfield, A.E., Hill, M.C., Rodell, M., Loomis, B.D., Stotler, R.L., Porter, M.E., 2018. In-Situ and GRACE-based Groundwater Observations : Similarities , Discrepancies , and Evaluation in the High Plains Aquifer in Kansas. Remote Sens. Environ. 205, 408–418. https://doi.org/10.1029/2018WR023836

Chen, T., Guestrin, C., 2016. XGBoost, in: Proceedings of the 22nd ACM SIGKDD International Conference on Knowledge Discovery and Data Mining. ACM, New York, NY, USA, pp. 785–794. https://doi.org/10.1145/2939672.2939785

Condon, L.E., Kollet, S., Bierkens, M.F.P., Fogg, G.E., Maxwell, R.M., Hill, M.C., Hendricks Fransen, H., Verhoef, A., Van Loon, A.F., Sulis, M., Abesser, C., 2021. Global groundwater modeling and monitoring: Opportunities and challenges. Water Resour. Res. 1–27. https://doi.org/10.1029/2020wr029500

Correia Filho, F., Andrade, J., Monteiro, A., Fontes, S., Feitosa, E., Soares Fillho, A., Sousa, N., Barradas, M., 2010. Aquífero Serra Grande: Hidrogeologia E Modelo Tectônico - Borda Sudeste Da Bacia Sedimentar Do Parnaíba - Pi. Rev. Águas Subterrâneas 0, 1–20.

Daubechies, I., 1992. Ten Lectures on Wavelets, in: Griffel, D.H. (Ed.), The Mathematical Gazette. p. 19. https://doi.org/10.2307/3620105

Diniz, J.A.O., Bomfim, L.F.C., Freitas, M.A. de, Monteiro, A.B., Cardoso, A. de C., Franzini, A.S., Aguiar, C.J.B. de, Silva, D.R.A. da, Santos, G.N. dos, Silva, H.R. da, Diniz, J.A.O., Machado, J.L.F., Martins, L.A., Pereira, L.A. da C., Galvão, M.J. da T.G., Memoriam), M.M. (in, Filho, O.A. de S., Araújo, P.P., Roberto, R.R.S., Kirchhein, E., Paula, T.L.F. de, 2014. Mapa Hidrogeológico do Brasil [WWW Document]. Serviço Geológico do Bras. URL http://www.cprm.gov.br/publique/Hidrologia/Estudos-Hidrologicos-e-Hidrogeologicos/Mapa-Hidrogeologico-do-Brasil-ao-Milionesimo-756.html (accessed 8.18.22).

Diniz, João Alberto O., Morais, F. De, Borba, Alexandre Luiz Borba Toian, G.C., 2012. Relatório Diagnóstico Aquífero Açu Bacia Sedimentar Potiguar.

Diniz, João Alberto Oliveira, Morais, F. de, Borba, A.L.S., Guilherme Casaroto, T., 2012. Relatório Diagnóstico Aquífero Tacaratu Bacia Sedimentar Jatobá. Belo Horisonte.

Ditmar, P., 2018. Conversion of time-varying Stokes coefficients into mass anomalies at the Earth's surface considering the Earth's oblateness. J. Geod. 92, 1401–1412. https://doi.org/10.1007/s00190-018-1128-0

Duchi, J.J., Singer, Y., 2011. Adaptive Subgradient Methods for Online Learning and Stochastic Optimization. J. Mach. Learn. Res. 12, 2121–2159.

Ebrahimi, H., Rajaee, T., 2017. Simulation of groundwater level variations using wavelet combined with neural network, linear regression and support vector machine. Glob. Planet. Change 148, 181–191. https://doi.org/10.1016/j.gloplacha.2016.11.014

Erkyihun, S.T., Rajagopalan, B., Zagona, E., Lall, U., Nowak, K., 2016. Wavelet-based time series bootstrap model for multidecadal streamflow simulation using climate indicators. Water Resour. Res. 52, 4061–4077. https://doi.org/10.1002/2016WR018696

Franzini, A.S., 2012. Sistema Aquífero Bauru-Caiuá Nos Estados De São Paulo, Mato Grosso Do Sul E Paraná, Levantamento De Recursos Hídricos Subterrâneos. São Paulo.

Frappart, F., Ramillien, G., 2018. Monitoring groundwater storage changes using the Gravity Recovery and Climate Experiment (GRACE) satellite mission: A review. Remote Sens. 10. https://doi.org/10.3390/rs10060829

Galvão, P.H.F., Demétrio, J.G.A., De Souza, E.L., Da Silva Pinheiro, C.D.S., Baessa, M.P.M., 2012. Hidrogeologia e geometria dos aquíferos das formações cretáceas Içá e Solimões, Bacia Paleozoica do Solimões, na região de Urucu, Amazonas. Rev. Bras. Geociencias 42, 142–153. https://doi.org/10.5327/Z0375-75362012000500012

Gaspar, M.T.P., Campos, J.E.G., 2007. O Sistema Aqüífero Urucuia. Rev. Bras. Geociências 37, 216–226.

Gaur, A., Simonovic, S.P., 2019. Introduction to Physical Scaling, in: Trends and Changes in Hydroclimatic Variables. Elsevier, pp. 199–273. https://doi.org/10.1016/B978-0-12-810985-4.00004-9

Gemitzi, A., Lakshmi, V., 2017. Downscaling GRACE data to estimate groundwater use at the aquifer scale, in: Proceedings of the 15th.

595 Géron, A., 2019. Hands-on Machine Learning whith Scikit-Learing, Keras and Tensorfow, 1st
596 ed, O'Reilly Media, Inc. O'Reilly Media, Inc, Boston.

597 Getirana, A., 2016. Extreme Water Deficit in Brazil Detected from Space. J. Hydrometeorol.
598 https://doi.org/10.1175/JHM-D-15-0096.1

599 Getirana, A., Jung, H.C., Arsenault, K., Shukla, S., Kumar, S., Peters-Lidard, C., Maigari, I.,
600 Mamane, B., 2020a. Satellite Gravimetry Improves Seasonal Streamflow Forecast
601 Initialization in Africa. Water Resour. Res. 56, 2019WR026259.
602 https://doi.org/10.1029/2019WR026259

603 Getirana, A., Libonati, R., Cataldi, M., 2021. Brazil is in water crisis — it needs a drought plan.
604 Nature 600, 218–220. https://doi.org/10.1038/d41586-021-03625-w

605 Getirana, A., Rodell, M., Kumar, S., Beaudoing, H.K., Arsenault, K., Zaitchik, B., Save, H.,
606 Bettadpur, S., 2020b. GRACE Improves Seasonal Groundwater Forecast Initialization over
607 the United States. J. Hydrometeorol. 21, 59–71. https://doi.org/10.1175/JHM-D-19-0096.1

608 Girotto, M., De Lannoy, G.J.M., Reichle, R.H., Rodell, M., Draper, C., Bhanja, S.N., Mukherjee,
609 A., 2017. Benefits and pitfalls of GRACE data assimilation: A case study of terrestrial water
610 storage depletion in India. Geophys. Res. Lett. 44, 4107–4115.
611 https://doi.org/10.1002/2017GL072994

612 Gonçalves, R.D., Stollberg, R., Weiss, H., Chang, H.K., 2020. Using GRACE to quantify the
613 depletion of terrestrial water storage in Northeastern Brazil: The Urucuia Aquifer System.
614 Sci. Total Environ. 705, 135845. https://doi.org/10.1016/j.scitotenv.2019.135845

615 Hinton, G., Srivastava, N., Swersky, K., 2012. Neural Networks for Machine Learning Lecture
616 6a Overview of mini---batch gradient descent [WWW Document]. URL
617 http://www.cs.toronto.edu/~tijmen/csc321/slides/lecture_slides_lec6.pdf (accessed
618 10.26.20).

619 Hu, K., Awange, J.L., Khandu, Forootan, E., Goncalves, R.M., Fleming, K., 2017.
620 Hydrogeological characterisation of groundwater over Brazil using remotely sensed and
621 model products. Sci. Total Environ. 599–600, 372–386.
622 https://doi.org/10.1016/j.scitotenv.2017.04.188

623 Huang, X., Gao, L., Crosbie, R.S., Zhang, N., Fu, G., Doble, R., 2019. Groundwater recharge
624 prediction using linear regression, multi-layer perception network, and deep learning. Water
625 (Switzerland) 11. https://doi.org/10.3390/w11091879

626 IBGE, I.B. de G. e E., 2020. Pesquisa Nacional de Saneamento Básico 2008, Ministério das
627 cidades. Rio de Janeiro.

628 Iqbal, N., Khan, A., Rizwan, A., Ahmad, R., Kim, B.W.A.N., Kim, K., Kim, D., 2021.
629 Groundwater Level Prediction Model Using Correlation and Difference Mechanisms Based
630 on Boreholes Data for Sustainable Hydraulic Resource Management. IEEE Access 9,
631 96092–96113. https://doi.org/10.1109/ACCESS.2021.3094735

632 Jung, H.C., Getirana, A., Arsenault, K.R., Kumar, S., Maigary, I., 2019. Improving surface soil
633 moisture estimates in West Africa through GRACE data assimilation. J. Hydrol. 575, 192–
634 201. https://doi.org/10.1016/j.jhydrol.2019.05.042

635 Ke, G., Meng, Q., Finley, T., Wang, T., Chen, W., Ma, W., Ye, Q., Liu, T.Y., 2017. LightGBM:
636 A highly efficient gradient boosting decision tree. Adv. Neural Inf. Process. Syst. 2017-
637 Decem, 3147–3155.

638 Khalil, B., Broda, S., Adamowski, J., Ozga-Zielinski, B., Donohoe, A., 2015. Short-term

639 forecasting of groundwater levels under conditions of mine-tailings recharge using wavelet
640 ensemble neural network models. Hydrogeol. J. 23, 121–141.
641 https://doi.org/10.1007/s10040-014-1204-3

642 Kingma, D.P., Ba, J.L., 2015. Adam: A method for stochastic optimization. 3rd Int. Conf. Learn.
643 Represent. ICLR 2015 - Conf. Track Proc. 1–15.

644 Klambauer, G., Unterthiner, T., Mayr, A., Hochreiter, S., 2017. Self-Normalizing Neural
645 Networks. Adv. Neural Inf. Process. Syst. 2017-Decem, 972–981.

646 Koster, R.D., Suarez, M.J., Ducharne, A., Stieglitz, M., Kumar, P., 2000. A catchment-based
647 approach to modeling land surface processes in a general circulation model: 1. Model
648 structure. J. Geophys. Res. Atmos. 105, 24809–24822.
649 https://doi.org/10.1029/2000JD900327

650 Kumar, S. V., Zaitchik, B.F., Peters-Lidard, C.D., Rodell, M., Reichle, R., Li, B., Jasinski, M.,
651 Mocko, D., Getirana, A., De Lannoy, G., Cosh, M.H., Hain, C.R., Anderson, M., Arsenault,
652 K.R., Xia, Y., Ek, M., 2016. Assimilation of Gridded GRACE terrestrial water storage
653 estimates in the North American land data assimilation system. J. Hydrometeorol. 17, 1951–
654 1972. https://doi.org/10.1175/JHM-D-15-0157.1

655 Lähivaara, T., Malehmir, A., Pasanen, A., Kärkkäinen, L., Huttunen, J.M.J., Hesthaven, J.S.,
656 2019. Estimation of groundwater storage from seismic data using deep learning. Geophys.
657 Prospect. 67, 2115–2126. https://doi.org/10.1111/1365-2478.12831

658 Lecun, Y., Bengio, Y., Hinton, G., 2015. Deep learning. Nature 521, 436–444.
659 https://doi.org/10.1038/nature14539

660 Li, B., Rodell, M., Kumar, S., Beaudoing, H.K., Getirana, A., Zaitchik, B.F., de Goncalves, L.G.,
661 Cossetin, C., Bhanja, S., Mukherjee, A., Tian, S., Tangdamrongsub, N., Long, D., Nanteza,
662 J., Lee, J., Policelli, F., Goni, I.B., Daira, D., Bila, M., de Lannoy, G., Mocko, D., Steele-
663 Dunne, S.C., Save, H., Bettadpur, S., 2019. Global GRACE Data Assimilation for
664 Groundwater and Drought Monitoring: Advances and Challenges. Water Resour. Res. 55.
665 https://doi.org/10.1029/2018WR024618

666 Liu, Y., Xia, X., Yao, L., Jing, W., Zhou, C., Huang, W., Li, Y., Yang, J., 2020. Downscaling
667 Satellite Retrieved Soil Moisture Using Regression Tree Based Machine Learning
668 Algorithms Over Southwest France. Earth Sp. Sci. 7.
669 https://doi.org/10.1029/2020EA001267

670 Manaswi, N.K., 2018. Regression to MLP in TensorFlow, in: Deep Learning with Applications
671 Using Python. Apress, Berkeley, CA, pp. 57–68. https://doi.org/10.1007/978-1-4842-3516-
672 4_4

673 Marcuzzo, F., Andrade, L., Melo, D., 2012. Métodos de Interpolação Matemática no Mapeamento
674 de Chuvas do Estado do Mato Grosso (Interpolation Methods in Mathematics of Rainfall
675 Mapping of the State of Mato Grosso). Rev. Bras. Geogr. Física 4, 793.
676 https://doi.org/10.26848/rbgf.v4i4.232714

677 Melati, M.D., Fleischmann, A.S., Fan, F.M., Paiva, R.C.D., Athayde, G.B., 2019. Estimates of
678 groundwater depletion under extreme drought in the Brazilian semi-arid region using
679 GRACE satellite data: application for a small-scale aquifer. Hydrogeol. J. 27, 2789–2802.
680 https://doi.org/10.1007/s10040-019-02065-1

681 Miro, M., Famiglietti, J., 2018. Downscaling GRACE Remote Sensing Datasets to High-
682 Resolution Groundwater Storage Change Maps of California's Central Valley. Remote
683 Sens. 10, 143. https://doi.org/10.3390/rs10010143

Moosavi, V., Vafakhah, M., Shirmohammadi, B., Behnia, N., 2013. A Wavelet-ANFIS Hybrid Model for Groundwater Level Forecasting for Different Prediction Periods. Water Resour. Manag. 27, 1301–1321. https://doi.org/10.1007/s11269-012-0239-2

Moosavi, V., Vafakhah, M., Shirmohammadi, B., Ranjbar, M., 2014. Optimization of Wavelet-ANFIS and Wavelet-ANN Hybrid Models by Taguchi Method for Groundwater Level Forecasting. Arab. J. Sci. Eng. 39, 1785–1796. https://doi.org/10.1007/s13369-013-0762-3

Mourão, M.A.A., 2009. Projeto - Implantação de Rede Integrada de Monitoramento das Águas Subterrâneas - Proposta Técnica. Belo Horisonte.

Nie, W., Zaitchik, B.F., Rodell, M., Kumar, S. V., Arsenault, K.R., Li, B., Getirana, A., 2019. Assimilating GRACE Into a Land Surface Model in the Presence of an Irrigation-Induced Groundwater Trend. Water Resour. Res. 55, 11274–11294. https://doi.org/10.1029/2019WR025363

Peixoto, D.D., Vasconcelos, T.E., Jamilo José, T.F., 2012a. Aquíferos Furnas e Vale Do Rio Do Peixe nos Estados de Mato Grosso e Goiás. Belo Horisonte.

Peixoto, D.D., Vasconcelos, T.E., Thomé Filho, J.J., 2012b. Relatório Diagnóstico Aquíferos Ronuro, Salto Das Nuvens e Utiariti no Estado do Mato Grosso, Bacia Sedimentar dos Parecis. Belo Horisonte.

Perktold, J., Seabold, S., Taylor, J., 2022. Statsmodels seasonal Decompose [WWW Document]. Statsmodels. URL https://www.statsmodels.org/dev/generated/statsmodels.tsa.seasonal.seasonal_decompose.html (accessed 1.14.22).

Prokhorenkova, L., Gusev, G., Vorobev, A., Dorogush, A.V., Gulin, A., 2017. CatBoost: unbiased boosting with categorical features. Adv. Neural Inf. Process. Syst. 2018-Decem, 6638–6648.

PyWavelets, 2022. Signal extension modes — PyWavelets Documentation [WWW Document]. URL https://pywavelets.readthedocs.io/en/latest/ref/signal-extension-modes.html (accessed 8.18.22).

Qi, X., Neupauer, R.M., 2008. Wavelet analysis of dominant scales of heterogeneous porous media 44, 9406. https://doi.org/10.1029/2006WR005720

Ramachandran, P., Zoph, B., Le Google Brain, Q. V, 2017. Searching For Activation Functions.

Ren, H., Song, X., Fang, Y., Hou, Z.J., Scheibe, T.D., 2021. Machine Learning Analysis of Hydrologic Exchange Flows and Transit Time Distributions in a Large Regulated River. Front. Artif. Intell. 4, 1–18. https://doi.org/10.3389/frai.2021.648071

Rhif, M., Abbes, A. Ben, Farah, I.R., Martínez, B., Sang, Y., 2019. Wavelet Transform Application for/in Non-Stationary Time-Series Analysis: A Review. https://doi.org/10.3390/app9071345

Richey, A.S., Thomas, B.F., Lo, M.-H., Reager, J.T., Famiglietti, J.S., Voss, K., Swenson, S., Rodell, M., 2015. Quantifying renewable groundwater stress with GRACE. Water Resour. Res. 51, 5217–5238. https://doi.org/10.1002/2015WR017349

Rodell, M., Famiglietti, J.S., Wiese, D.N., Reager, J.T., Beaudoing, H.K., Landerer, F.W., Lo, M.-H., 2018. Emerging trends in global freshwater availability. Nature 557, 651–659. https://doi.org/10.1038/s41586-018-0123-1

Rodell, M, Houser, P.R., Jambor, U., Gottschalck, J., Mitchell, K., Meng, C.-J., Arsenault, K.,

Cosgrove, B., Radakovich, J., Bosilovich, M., Entin, J.K., Walker, J.P., Lohmann, D., Toll, D., Rodell, Matthew, 2003. THE GLOBAL LAND DATA ASSIMILATION SYSTEM. https://doi.org/10.1

Rowlands, D.D., Luthcke, S.B., McCarthy, J.J., Klosko, S.M., Chinn, D.S., Lemoine, F.G., Boy, J.-P., Sabaka, T.J., 2010. Global mass flux solutions from GRACE: A comparison of parameter estimation strategies—Mass concentrations versus Stokes coefficients. J. Geophys. Res. 115, B01403. https://doi.org/10.1029/2009JB006546

Santos, L.C.A. dos, 2005. Reflexões sobre água subterrânea do estado do maranhão, Universidade Estadual do Maranhão. São Luiz.

Save, H., 2022. CSR GRACE and GRACE-FO RL06 Mascon Solutions v02 [WWW Document]. Cent. Sp. Res. URL http://www2.csr.utexas.edu/grace/RL06_mascons.html (accessed 2.1.22).

Save, H., Bettadpur, S., Tapley, B.D., 2016. High-resolution CSR GRACE RL05 mascons. J. Geophys. Res. Solid Earth 121, 7547–7569. https://doi.org/10.1002/2016JB013007

Scanlon, B.R., Longuevergne, L., Long, D., 2012. Ground referencing GRACE satellite estimates of groundwater storage changes in the California Central Valley, USA. Water Resour. Res. 48. https://doi.org/10.1029/2011WR011312

Scanlon, B.R., Zhang, Z., Save, H., Sun, A.Y., Müller Schmied, H., van Beek, L.P.H., Wiese, D.N., Wada, Y., Long, D., Reedy, R.C., Longuevergne, L., Döll, P., Bierkens, M.F.P., 2018. Global models underestimate large decadal declining and rising water storage trends relative to GRACE satellite data. Proc. Natl. Acad. Sci. 115. https://doi.org/10.1073/pnas.1704665115

Scikit-learn, 2021. Scikit-learn: machine learning in Python — scikit-learn 1.0.2 documentation [WWW Document]. Scikit-learn. URL https://scikit-learn.org/stable/index.html (accessed 1.11.22).

Sehgal, V., Gaur, N., Mohanty, B.P., 2021. Global Flash Drought Monitoring Using Surface Soil Moisture. Water Resour. Res. 57, 1–32. https://doi.org/10.1029/2021WR029901

Siebert, S., Burke, J., Faures, J.M., Frenken, K., Hoogeveen, J., Döll, P., Portmann, F.T., 2010. Groundwater use for irrigation - A global inventory. Hydrol. Earth Syst. Sci. 14, 1863–1880. https://doi.org/10.5194/hess-14-1863-2010

Silva, T.M.G. da, 2013. Caracterização do Sistema Aquífero Parecis na região Centro-Norte do estado de Mato Grosso : subsídios para a gestão dos recursos hídricos subterrâneos. UNB.

Silva, S., Monteiro, A., Cabral, J., Borba, A., Freire, P., Costa, W., Barbosa, G., 2008. A Gestão De Águas Subterrâneas No Aqüífero Barreiras – Jordão, Jardim Jordão E Ibura – Recife – Pernambuco. Rev. Águas Subterrâneas 0, 1–18.

Sklearn, 2022. sklearn.model_selection.KFold — scikit-learn 1.0.2 documentation [WWW Document]. Sklearn. URL https://scikit-learn.org/stable/modules/generated/sklearn.model_selection.KFold.html (accessed 1.31.22).

Souza, C.D. de, Castro, M.A.H. de, 2013. Simulação do fluxo hídrico subterrâneo por estimativa de parâmetros usando cargas hidráulicas observadas: caso do Cariri Cearense, Brasil. Rev. Recur. Hídricos 34, 43–61. https://doi.org/10.5894/rh34n1-4

Stollnitz, E.J., DeRose, A.D., Salesin, D.H., 1995. Wavelets for computer graphics: a primer.1. IEEE Comput. Graph. Appl. 15, 76–84. https://doi.org/10.1109/38.376616

771 Sun, A.Y., 2013. Predicting groundwater level changes using GRACE data. Water Resour. Res.
772 49, 5900–5912. https://doi.org/10.1002/wrcr.20421

773 Sun, A.Y., Scanlon, B.R., Zhang, Z., Walling, D., Bhanja, S.N., Mukherjee, A., Zhong, Z., 2019.
774 Combining Physically Based Modeling and Deep Learning for Fusing GRACE Satellite
775 Data: Can We Learn From Mismatch? Water Resour. Res. 55, 1179–1195.
776 https://doi.org/10.1029/2018WR023333

777 Swenson, S., Wahr, J., Milly, P.C.D., 2003. Estimated accuracies of regional water storage
778 variations inferred from the Gravity Recovery and Climate Experiment (GRACE). Water
779 Resour. Res. https://doi.org/10.1029/2002WR001808

780 Takahashi, A.T., 2012. Projeto Rede Integrada de Monitoramento das Águas Subterrâneas:
781 Sistema Aquífero Guarani Nos Estados De São Paulo, Mato Grosso Do Sul E Paraná
782 [Takahashi, A.T. e Mourão, M.A.A. Coord.], Levantamento De Recursos Hídricos
783 Subterrâneos. São Paulo.

784 Tao, H., Hameed, M.M., Marhoon, H.A., Zounemat-Kermani, M., Heddam, S., Kim, S.,
785 Sulaiman, S.O., Tan, M.L., Sa'adi, Z., Mehr, A.D., Allawi, M.F., Abba, S., Zain, J.M.,
786 Falah, M.W., Jamei, M., Bokde, N.D., Bayatvarkeshi, M., Al-Mukhtar, M., Bhagat, S.K.,
787 Tiyasha, T., Khedher, K.M., Al-Ansari, N., Shahid, S., Yaseen, Z.M., 2022. Groundwater
788 level prediction using machine learning models: A comprehensive review. Neurocomputing
789 489, 271–308. https://doi.org/10.1016/j.neucom.2022.03.014

790 Tapley, B., Bettadpur, S., Watkins, M., Reigber, C., 2004. The gravity recovery and climate
791 experiment: Mission overview and early results. Geophys. Res. Lett. 31, 1–4.
792 https://doi.org/10.1029/2004GL019920

793 Torrence, C., Compo, G.P., 1998. A Practical Guide to Wavelet Analysis. Bull. Am. Meteorol.
794 Soc. 79, 61–78. https://doi.org/10.1175/1520-0477(1998)079<0061:APGTWA>2.0.CO;2

795 UNESCO, 2020. Groundwater [WWW Document]. URL https://en.unesco.org/themes/water-
796 security/hydrology/groundwater (accessed 2.22.21).

797 Yin, W., Hu, L., Zhang, M., Wang, J., Han, S.C., 2018. Statistical Downscaling of GRACE-
798 Derived Groundwater Storage Using ET Data in the North China Plain. J. Geophys. Res.
799 Atmos. 123. https://doi.org/10.1029/2017JD027468

800 Yosefvand, F., Shabanlou, S., 2020. Forecasting of Groundwater Level Using Ensemble Hybrid
801 Wavelet–Self-adaptive Extreme Learning Machine-Based Models. Nat. Resour. Res. 29,
802 3215–3232. https://doi.org/10.1007/s11053-020-09642-2

803 Zare, M., Koch, M., 2018. Groundwater level fluctuations simulation and prediction by ANFIS-
804 and hybrid Wavelet-ANFIS/Fuzzy C-Means (FCM) clustering models: Application to the
805 Miandarband plain. J. Hydro-environment Res. 18, 63–76.
806 https://doi.org/10.1016/j.jher.2017.11.004

807 Zhang, G., Zheng, W., Yin, W., Lei, W., 2020. Improving the Resolution and Accuracy of
808 Groundwater Level Anomalies Using the Machine Learning-Based Fusion Model in the
809 North China Plain. Sensors 21, 46. https://doi.org/10.3390/s21010046

Tables and Figures

Table 1 – Effective porosity in Brazilian aquifers.

Aquifer	Effective porosity (S_y)	Reference
Açu	0.10	(Diniz et al., 2012)
Alter do Chão	0.18	(Aguiar & Mourão, 2012)
Areado	0.05	Estimated
Barreiras (Pirabas e Grajau)	0.10	(Silva et al., 2008)
Caiuá	0.17	(Franzini, 2012)
Beberibe	0.10	(Silva et al., 2008)
Boa Vista	0.18	Estimated
Cabeças	0.03	(Correia Filho et al., 2010)
Cenozoic Covers Aquifer	0.10	Estimated
Furnas	0.13	(Peixoto et al., 2012a)
Guarani	0.18	(Takahashi, 2012)
Iça	0.10	(Galvão et al., 2012)
Itapecuru	0.13	(Santos, 2005)
Coastal	0.14	Estimated
Missão/Velha-Mauriti	0.10	(Souza and Castro, 2013)
Parecis	0.15	(Silva, 2013)
Poti Piauí	0.15	(Correia Filho et al., 2010)
Prosperança	0.15	(Peixoto et al., 2012b)
Ronuro	0.12	(Peixoto et al., 2012b)
Salto das Nuvens	0.13	(Peixoto et al., 2012b)
Serra do Tucano	0.17	Estimated
Serra Grande	0.03	(Aguiar, 2017)
Tacaratu	0.03	(Diniz et al., 2012)
Trombetas	0.15	Estimated
Tucunare	0.10	Estimated
Urucuia	0.13	(Gaspar and Campos, 2007)

Table 2 - Results of the E3 and E4 experiments for Brazilian aquifers.

Aquifer		Wells	Correlation RIMAS x GRACE	RMSE (cm) GWS_{SIM}	MAE(cm) GWS_{SIM}	NSE GWS_{SIM}	RMSE (cm) GWS_{CLSM}	MAE(cm) GWS_{CLSM}
Guarani	Exp. 3	Train	-0.305	1.651	1.430	0.63	3.629	2.802
		Test	-0.529	1.492	1.044	-	-	-
	Exp. 4	Train	-0.312	2.351	1.535	0.63	5.958	4.562
		Test	-0.134	3.168	2.309	-	-	-
Bauru-Caiuá	Exp. 3	Train	-0.394	1.520	0.894	0.84	6.662	5.492
		Test	-0.367	2.502	1.660	-	-	-
	Exp. 4	Train	-0.408	1.911	1.120	0.85	6.854	5.375
		Test	-0.411	1.100	1.934	-	-	-
Parecis	Exp. 3	Train	-0.569	1.733	1.207	0.84	9.680	8.224
		Test	-0.59	3.104	2.493	-	-	-
	Exp. 4	Train	-0.445	2.412	1.361	0.90	9.118	6.984
		Test	-0.417	2.979	2.368	-	-	-
Urucuia	Exp. 3	Train	-0.153	0.705	0.37	0.88	2.812	2.124
		Test	-0.411	1.593	0.95	-	-	-
	Exp. 4	Train	-0.178	0.645	0.361	0.74	3.247	2.440
		Test	-0.108	1.431	1.015	-	-	-
Cabeças	Exp. 3	Train	-0.229	0.216	0.123	0.92	5.541	4.427
		Test	-0.465	0.88	0.597	-	-	-
	Exp.4	Train	-0.049	0.412	0.34	0.73	5.543	4.271
		Test	-0.297	0.668	0.47	-	-	-
Alter do Chão	Exp. 4	Train	-0.028	3.114	2.364	0.89	9.749	7.601
		Test	0.187	7.265	5.940	-	-	-
Araripe	Exp. 4	Train	-0.205	0.240	0.880	0.88	2.161	1.519
		Test	-0.302	2.127	1.714	-	-	-
Iça	Exp. 4	Train	-0.043	1.112	0.685	0.91	4.237	3.131
		Test	-0.01	4.936	3.733	-	-	-

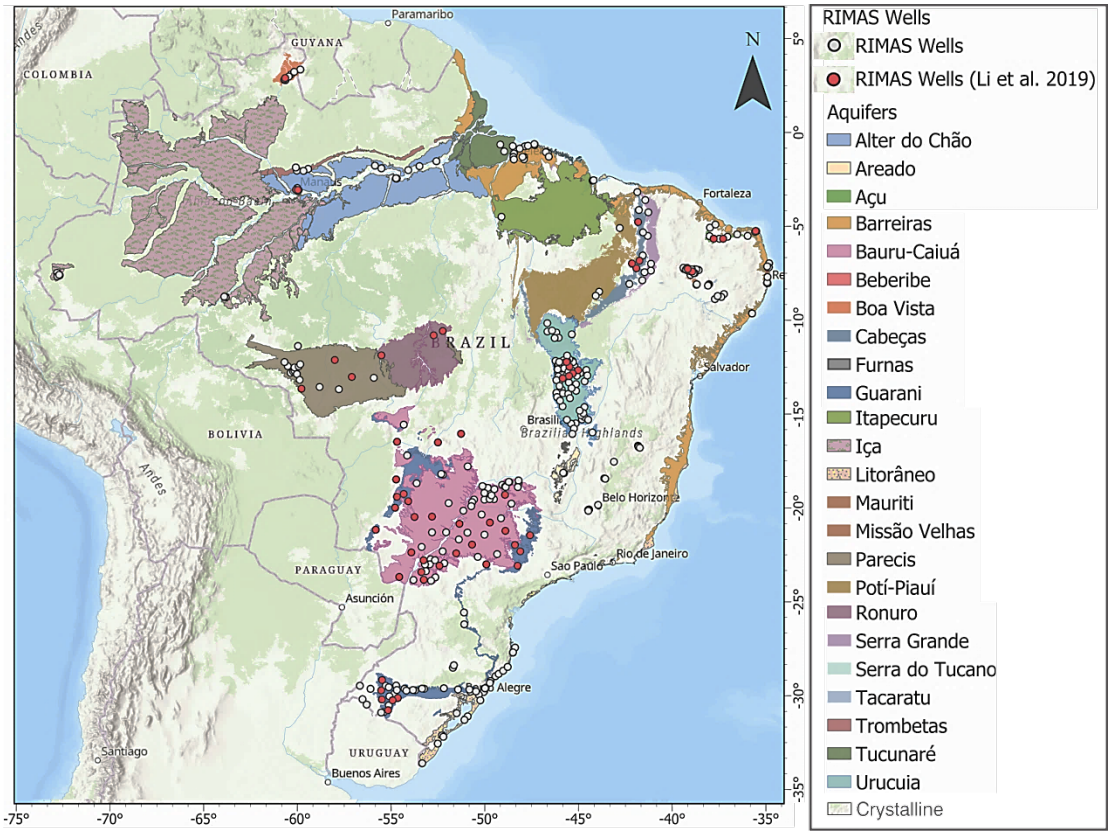

Figure 1 - Geographical location of Brazilian aquifers and spatial distribution of the RIMAS groundwater monitoring network. RIMAS wells colored in red are those used in Li et al. (2019).

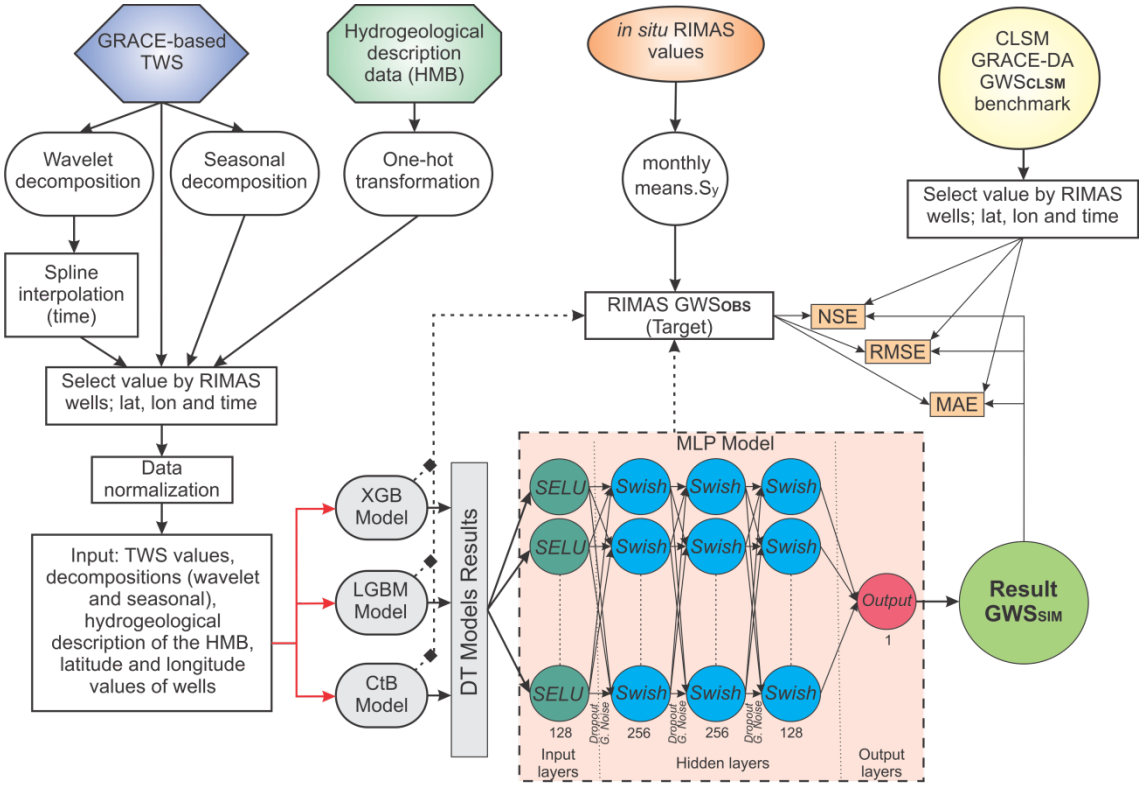

819

820

821 **Figure 2** - Processing flow diagram and ensemble model architecture. It should be emphasized
822 that both the DT models and the MLP model target the GWS_{OBS}, values observed in the RIMAS
823 wells.

824

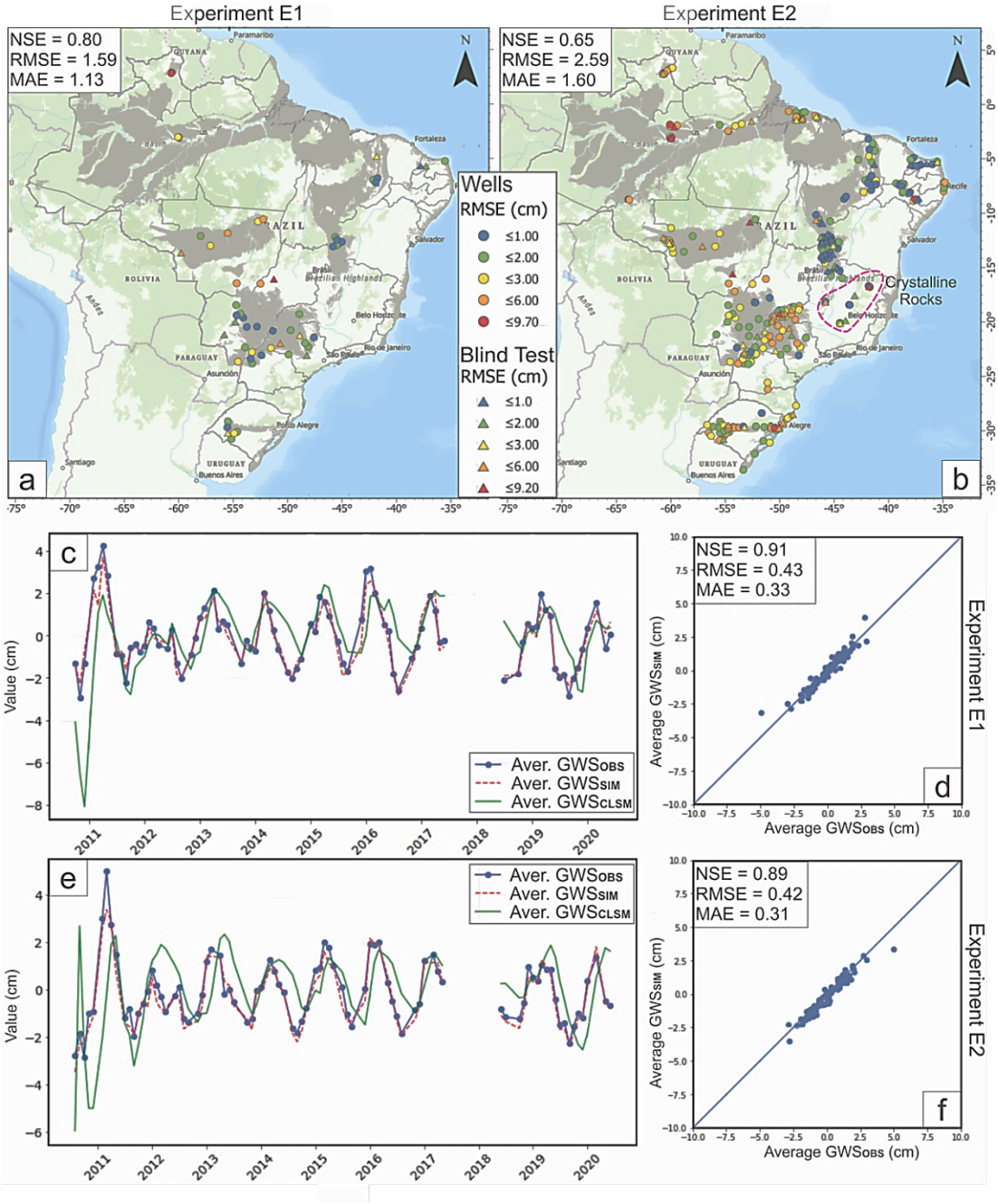

825

826 **Figure 3** – Experimental results for E1 and E2: (a) RMSE (cm) mapping of the forecast model
827 set for the wells used in Li et al. (2019) and statistical metrics of the model for the data set used;
828 (b) RMSE (cm) mapping of all RIMAS wells in Brazil and model metrics for the dataset used,
829 highlighted area of crystalline rocks; (c), (e) graphs of the average results GWS, E1 and E2, for
830 the observed values (GWS_{OBS}), simulated (GWS_{SIM}) and obtained from CLSM (GWS_{CLSM}); and
831 (d), (f) values of NSE, RMSE and MAE for the means of the results of E1 and E2.

832

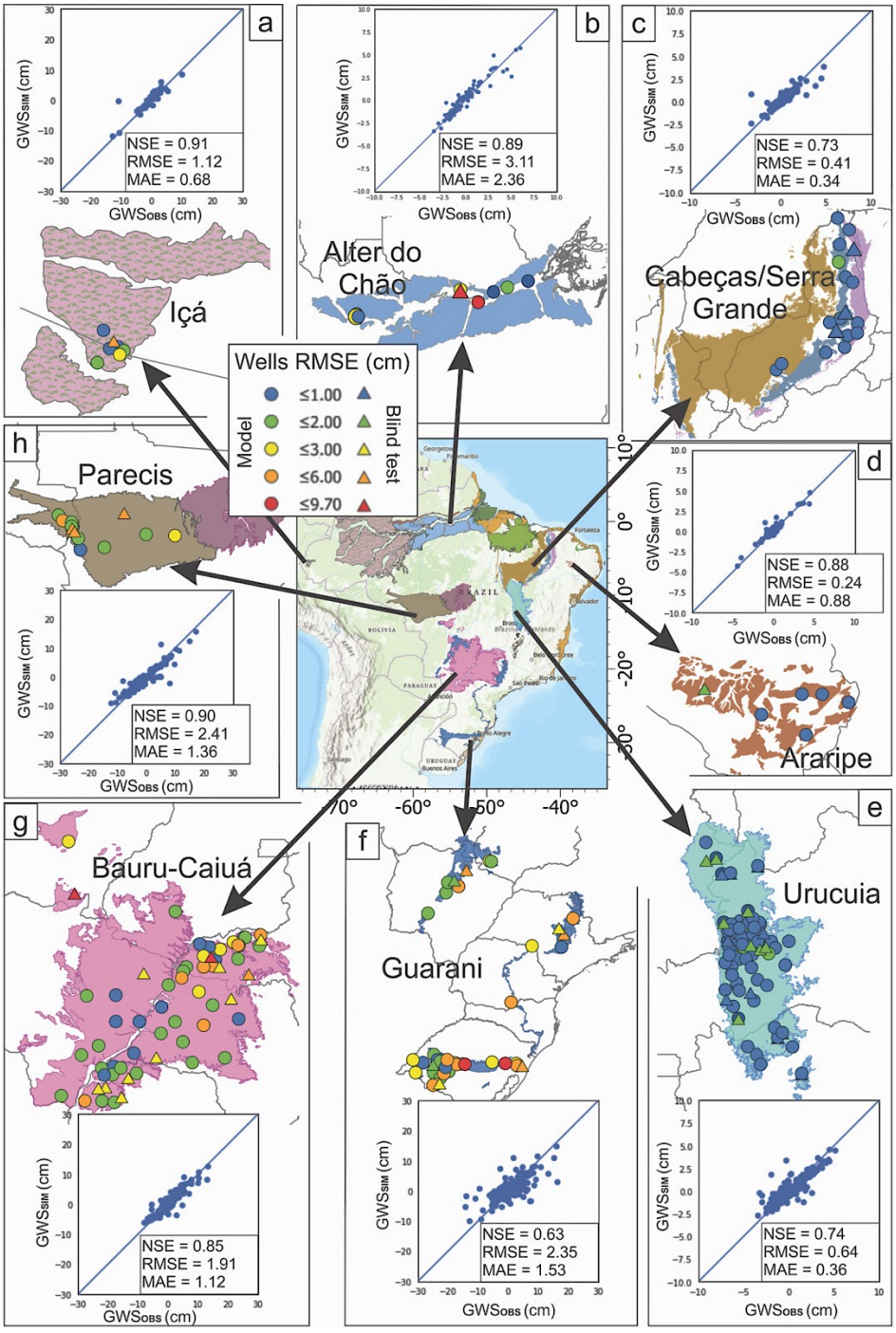

Figure 4 – Results for experiments E4: RMSE (cm) mapping for Içá, Alter do Chão and Parecis aquifers, featuring wells inserted in an Equatorial climate and with great contribution of surface water in the TWS response (a, b and h); RMSE (cm) mapping for Cabeças, Serra Grande, Poti aquifers (Cabeças/Serra Grande), Missão Velha and Mauriti (Araripe) and Urucuia, a region of great exploitation of groundwater, inserted in a semi-arid climate (c, d and e); RMSE (cm) mapping for Guarani and Bauru-Caiuá aquifers, region of intense exploitation of groundwater and tropical climate (f and g). The scatter plots represent the 20% simulated test values (GWS_{SIM}) and observed values (GWS_{OBS}), in each aquifer.

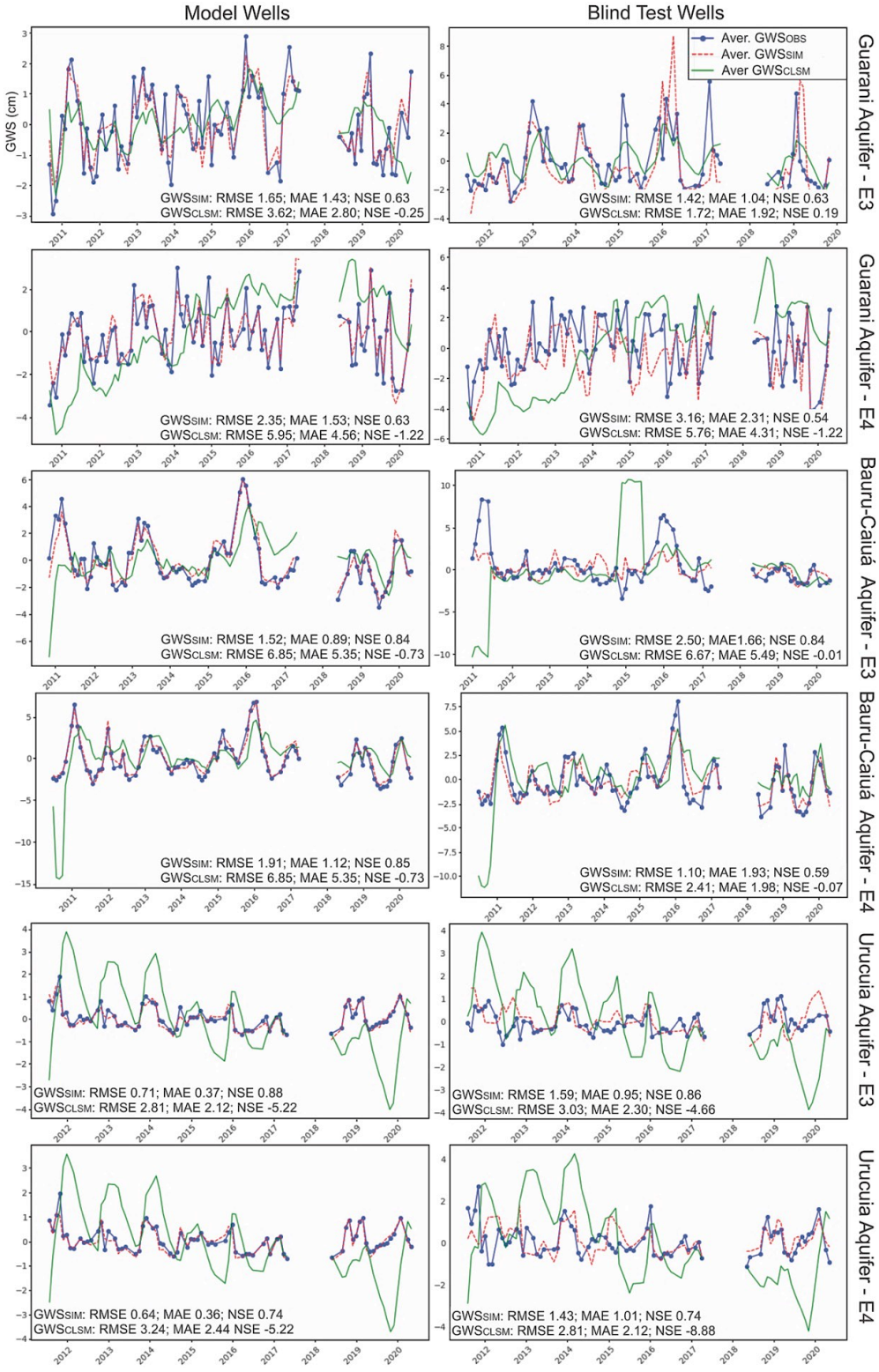

Figure 5 - Average results of the GWS for the experiments E3 and E4, in the Guarani, Bauru-Caiuá and Urucuia aquifers, considering *in situ* values (GWS_{OBS}), forecasted values (GWS_{SIM}) and CLSM results (GWS_{CLSM}). RMSE [cm], MAE [cm] and NSE [-] values for both GWS_{SIM} and GWS_{CLSM} are also provided.